QUANTIFYING COLLAGEN-BASED BIOLOGICAL TISSUES USING FOURIER TRANSFORM-SECOND-HARMONIC GENERATION IMAGING

BY

TUNG YUEN LAU

THESIS

Submitted in partial fulfillment of the requirements
for the degree of Master of Science in Mechanical Engineering
in the Graduate College of the
University of Illinois at Urbana-Champaign, 2013

Urbana, Illinois

Advisor:

Associate Professor Kimani C. Toussaint, Jr.

ABSTRACT

The purpose of this thesis is to report the generalization of Fourier transform-second-harmonic generation (FT-SHG) imaging to quantify the arrangement of collagen fibers in biological tissues in 3D. Collagen is the primary structural protein in the human body. Depending on the spatial arrangement of collagen fibers, collagen-based biological tissues can have a wide range of functions and mechanical properties. In addition, many biological tissues consist of 3D hierarchical structures made of collagen. Therefore, a 3D quantitative imaging technique with high specificity to collagen fibers will be a valuable tool for diagnostic and medical purposes. Recently, we have generalized FT-SHG to 3D by utilizing the 3D imaging capability of SHG microscopy and combining that with 3D spatial Fourier analysis to quantify collagen fiber organization. Via 3D FT-SHG, quantitative metrics such as orientation isotropy and preferred orientation can be extracted readily from SHG images. This thesis is going to demonstrate the utility of 3D FT-SHG by apply it to three different biological tissues: porcine tendon, porcine sclera, and rat cervix.

ACKNOWLEDGEMENTS

I wish to express my most sincere appreciation to my advisor, Professor Kimani C. Toussaint Jr. Because of him, I fully understand the importance of diligence and integrity. Without the support and guidance he has given me for the past two years, I would not have achieved what I have accomplished today. A special thank to Dr. Raghu Ambekar for helping me start at the PROBE lab. He is a great mentor and an excellent colleague. I would also like the thank the members of PROBE Lab: Santosh Tripahti, Brian Roxworthy, Mehdi Zaman, Mahfuz Kabir, Abdul Bhuiya, and Dr. Hao Chen for their friendship and support. Finally I would like to acknowledge my family for giving me strength and encouragement.

Table of Contents

1 Introduction **1**
1.1 Overview 1
1.2 Organization of chapters 3

2 Background **4**
2.1 Motivation 4
2.2 Second-harmonic generation imaging 5
2.3 Fourier transform-second-harmonic generation imaging 8

3 Development of 3D FT-SHG **10**
3.1 Introduction 10
3.2 Methods 13
3.3 Results and discussion 17
3.4 Conclusion 26

4 Application of FT-SHG to rat cervical tissues **27**
4.1 Introduction 27
4.2 Methods 29
4.3 Results and discussion 32
4.4 Conclusion 41

5 Conclusion **43**

References **45**

Chapter 1

Introduction

1.1 Overview

Collagen is an important structural protein that it accounts for approximately 25% of the total protein mass [1, 2]. Fibrous collagen, such as type I collagen, is a tough material as its primary function is to bear loads. Depending on the spatial arrangement of collagen fibers, collagen can achieve a wide range of mechanical properties. For instance, it provides flexibility in skin, and improves stiffness and maintains shapes in bone. Therefore, the quantification of the spatial arrangement of collagen fibers is an important part of studying mechanical properties and functions of biological tissues. Another important characteristic of collagen is that collagen-based tissues are prone to alter due to diseases and injuries [3–9]. For example, recent studies in human breast cancer have shown significant differences in the spatial arrangement of collagen fibers between normal and malignant tissues [4, 7]. Therefore, the ability to monitor changes in the spatial arrangement of collagen fibers is essential to evaluate the health status of a

particular tissue, and to develop tools for medical applications.

Among many imaging techniques, second-harmonic generation (SHG) microscopy provides a perfect platform for imaging collagen-based tissues because of its high specificity to collagen fibers and minimally invasive requirements for sample preparation. SHG is a nonlinear optical process that the generation of signals is due to nonlinear scattering within a non-centrosymmetric material. Since fibrous collagen (e.g. type I collagen) is non-centrosymmetric; therefore, high contrast images of collagen fibers can be imaged without the need for exogenous staining. In addition, since SHG is a scattering process that no energy is absorbed by the sample during imaging, it is low in photo-toxicity in comparison with conventional fluorescence imaging. In the past decade, SHG microscopy has become a popular technique for imaging collagen fibers in biological tissues, and there has been much effort on developing quantitative metrics for SHG imaging. Fourier transform-second-harmonic generation (FT-SHG) imaging is a technique that combines SHG microscopy with spatial Fourier analysis to quantify collagen fiber arrangement. By applying spatial Fourier analysis to SHG images, quantitative parameters such as orientation isotropy and preferred orientations of collagen fibers inside a biological tissue can be extracted readily. In our early studies, FT-SHG was applied to extract spatial information from 2D SHG images [3, 4, 10–12]. Since most biological tissues contain 3D fibrillar structures, a 3D quantitative technique may offer more utility. Therefore, we have generalized FT-SHG to 3D in our recent stud-

ies [13–15].

1.2 Organization of chapters

This thesis focuses on the generalization and the application of Fourier transform-second-harmonic generation (FT-SHG) imaging to quantify collagen fiber arrangement in biological tissues in 3D. Chapter 2 outlines the motivation and the background of applying FT-SHG to quantify biological tissues. Chapter 3 focuses on the generalization of FT-SHG to quantify collagen fiber organization in 3D. It includes the methodology of 3D FT-SHG, a comparative analysis of 2D and 3D FT-SHG, as well as example applications to porcine tendon and sclera tissues. Chapter 4 discusses the recent application of FT-SHG to quantify rat cervical tissues from both 2D and 3D perspectives. Chapter 5 is the general conclusion of this thesis.

Chapter 2

Background

2.1 Motivation

Collagen is the most abundant protein in vertebrates [1, 2]. In fact, it accounts for approximately 25% of the total protein mass in mammals [1, 2]. It is a fibrous and insoluble protein that can be found at the extracellular matrix (ECM) of most tissues (e.g. cornea, tendon, bone, skin, etc.) [1–4, 11, 12, 16, 17]. In the human body, there are 20 types of collagen, and the most common collagen is type I collagen. Type I collagen is a strong fibrillar material that its primary function is to withstand loads. Depending on the spatial arrangement of collagen fibers, tissues that contain collagen can have a wide range of mechanical properties. For instance, collagen fibers are arranged as parallel bundles known as fascicles in tendon to withstand axial tension and, at the same time, to provide enough flexibility for movement. Another example is the spatial arrangement of collagen fibers in bone. Bone is a functionally graded material that the spatial arrangement of ma-

terials changes over its volume. In cortical bone, where the structure is more compact, collagen fibers are packed tightly and concentrically around each osteon [12, 18, 19]. In trabecular bone, however, fibers are oriented along the longitudinal direction of the trabeculae such that loads can be transmitted from the diaphysis to the joint along the spongy bone framework in the epiphysis [18, 19]. Therefore, the quantification of the spatial organization of collagen fibers in biological tissues is essential for studying their mechanical properties and functions.

2.2 Second-harmonic generation imaging

Second-harmonic generation (SHG) is a nonlinear optics phenomenon. It is a special case of sum-frequency generation, where the two input photons of the same frequency are annihilated simultaneously and an output photon with twice the frequency is generated [fig. 2.1]. The requirements of efficient SHG are a high intensity input field and a non-centrosymmetric sample. A high intensity field increases the probability of SHG. A non-centrosymmetric materials has a nonzero second-order susceptibility tensor, which is essential for SHG. Since SHG is a scattering process that the generation of the output photon is from a virtual-state-to-ground-state transition rather than from an excited-state-to-ground-state transition (as is the case with fluorescence), and as such, no energy is absorbed during the process [fig. 2.2]. Therefore, it has low photo-toxicity in comparison with fluorescence imaging. In addition, since the generation of contrast is due to SHG from a non-centrosymmetric

material, high contrast images of fibrillar biological tissues can be imaged via SHG microscopy without the need for exogenous staining. Moreover, since SHG is a nonlinear optical process, the intensity of SHG signal varies quadratically with the intensity of the input optical field. In the case of using a highly focused pulsed laser beam, the generation of signal is limited to a sub-femtoliter focal volume; therefore, SHG microscopy is intrinsically confocal that it permits 3D imaging. Based on that, the arrangement of collagen fibers inside a biological tissue can be observed in more details from a 3D perspective. Because of its minimally invasive requirements for sample preparation, high specificity, and 3D imaging capability, SHG microscopy has become an increasingly popular technique for imaging collagen-based biological materials.

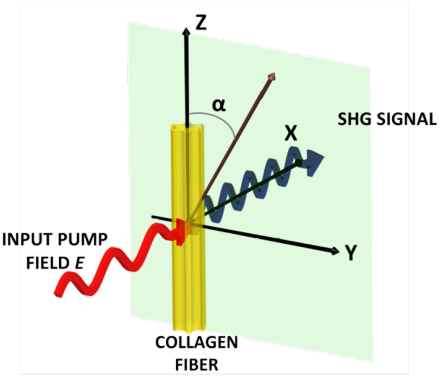

Figure 2.1: The schematic of second harmonic generation in a non-centrosymmetric collagen fiber [4].

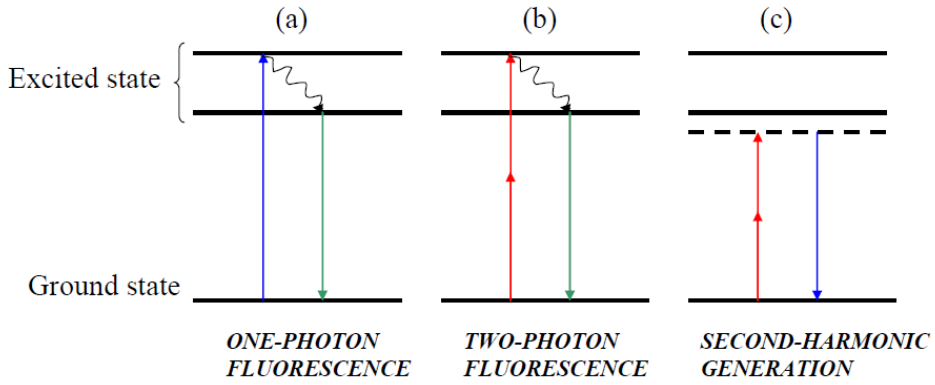

Figure 2.2: The Jablonski diagrams of a) one-photon fluorescence, b) two-photon fluorescence, and c) second-harmonic generation [20].

In recent years, there has been much effort on the development of quantitative SHG microscopy. Metrics such as forward-to-backward SHG signal intensity ratio and polarization-SHG provide information about the ionic environment of a tissue and alteration in collagen molecules, respectively [4, 10, 11, 21–25]. Other metrics such as orientation isotropy and preferred orientation focus on quantifying the spatial arrangement of collagen fibers. The later was found to be of special interest to researches on the bio-mechanical properties of various tissues [3, 17]. FT-SHG, whereby the unique process of SHG imaging is combined with spatial Fourier analysis, enables quantitative information of a collagen based tissue to be extracted readily. In the following section, we will discuss the background of FT-SHG in more details.

2.3 Fourier transform-second-harmonic generation imaging

Fourier transform is a well-developed mathematical tool that has been applied to various areas to analyze signals and images. In image processing, spatial Fourier analysis breaks down an image into a superposition of sinusoids of different frequencies, amplitudes, phases, and orientations. It is well-known that spatial orientation and its corresponding spread (orientation isotropy) calculated from the Fourier domain provides more general information about the overall morphology of the image. In addition, it is a simple technique that images can be analyzed easily without the need for complex algorithms. Therefore, quantitative information can be extracted readily using Fourier analysis. By combining SHG imaging with spatial Fourier analysis, we have developed Fourier transform-second-harmonic generation (FT-SHG) imaging to evaluate collagen-based materials.

Our early studies have demonstrated the utility of FT-SHG in quantifying spatial arrangement of collagen fibers by applying Fourier analysis to 2D SHG images. We have quantified the structural organization of collagen fibers using parameters such as, fiber orientation, spacing, and thickness [3, 4, 11, 12, 16, 17, 26, 27]. Additionally, our algorithm is able to label local regions based on the local orientation isotropy and average pixel intensity [13]. The applications of 2D FT-SHG to assess injuries in horse tendon, to explore age-related changes in porcine cortical bone, and to detect spatial differences in collagen fiber arrangement between normal and malignant

human breast tissues have shown promising potential to biomedical applications. Still, there are many problems in biology that would benefit from the analysis of the spatial organization of collagen fibers in 3D due to the fact that many biological tissues consist of 3D hierarchical structures made of collagen fibers. Therefore, we have generalized our technique to quantify collagen fiber organization in 3D.

Chapter 3

Development of 3D FT-SHG

3.1 Introduction

3.1.1 Motivation

As mentioned in the previous chapter, SHG microscopy is an increasing popular technique due to its ability to generate high contrast images of fibrillar collagen-based biological tissues without the need for staining [3, 11, 24, 28, 29]. Recent studies that utilize SHG microscopy have shown that unwanted alterations in collagen fiber arrangements are often associated with diseases or injuries [3–9]. For instance, bone tissues that suffer from osteogenesis imperfecta, a structural disorder that leads to brittleness and reduction in bone strength, contain reduced collagen content and increased proportion of nonlamellar collagen structure [12, 22, 30, 31]. Another representative example is the presence of highly ordered, yet unevenly-distributed collagen fibers in malignant tissues observed using SHG microscopy [5, 32, 33]. Such spatial

alterations may provide cues to the migration of malignant cells during cancer progression [8,33]. In addition, collagen fiber organization is responsible for structural roles and functions of biological tissues [17,19,30,34,35]. For example, collagen fibers form a functionally graded structure in cartilage to provide support, cushioning, and lubrication [26,27,36]. Moreover, the optical transparency and flexibility of cornea were shown to be dependent on the orientation of the embedded collagen fibers [17,37–40]. Therefore, quantitative SHG imaging of collagen fibers would be of great interest to medical and bioengineering applications.

3.1.2 Background

For the evaluation of fibrillar structures in biological tissues, there has been much effort on developing metrics to quantify SHG images [21,29,38]. For the assessment of spatial arrangements, parameters such as fiber orientation, spacing, and thickness are often employed [29,40,41]. Such parameters can be obtained from both the spatial domain and the frequency domain. Using a computational approach, measurements can be performed more objectively and quickly. Image processing techniques, such as the Hough transform, Fourier analysis, and principle component analysis are often applied to extract spatial information from 2D images [11,29,42–46]. Such methods are useful for analyzing images globally, and the computational cost is invariant to the complexity of the image. In contrast, bottom-up techniques such as fiber tracing and center-line extraction can provide localized information

regarding the dimension and orientation of a particular fiber [47–49]. In addition, bottom-up techniques are often applied to diffusion tensor imaging of nerve fibers and muscle fibers [48, 50–54]. Some recent studies have also applied fiber tracing to analyze the 3D orientation and branching of collagen fibers in collagen gels and cornea [40, 49, 55]. However, the performance and computational cost of bottom-up methods strongly depend on the complexity of the image (fiber population, density, and length) [51]; bottom-up methods are not feasible for application to, for example, dense fibrillar tissues. Therefore, to study the overall morphology of collagen fibers in biological tissues, methods such as the spatial Fourier transform offer more utility.

3.1.3 FT-SHG

Our early studies in Fourier transform-second harmonic generation (FT-SHG) imaging utilizes 2D spatial Fourier analysis to quantify the structural organization of collagen fibers using parameters such as, fiber orientation, spacing, and thickness [3, 10–12, 29]. Additionally, our technique labels regions of an image based on local orientation isotropy and average pixel intensity [3, 12]. The applications to assess injuries in horse tendon and age-related growth in porcine cortical bone have shown promising potential to utilize FT-SHG for important biomedical problems [3, 12]. Still, there are many problems in biology that would benefit from understanding the spatial organization of collagen fibers in 3D. For example, recent research

on collagenous fibrosis has shown that pathological changes due to fibrosis progression are depicted more precisely through 3D analysis [23, 37, 56, 57]. Therefore, we have generalized FT-SHG to quantify collagen fiber organization in 3D.

This chapter is going to discussion the generalization of FT-SHG to 3D. Section 2 of this chapter is going to explain the methodology of 3D FT-SHG, including sample preparation, image acquisition, image processing, and 3D Fourier orientation analysis. Example applications to porcine sclera and porcine tendon, and a comparative analysis of 2D and 3D FT-SHG are provided in section 3. We conclude in section 4 with a brief summary.

3.2 Methods

3.2.1 Sample Preparation

Porcine tissue samples of sclera and tendon were obtained from a local slaughter house after euthanasia, and stored immediately in 10% formalin. Smaller tissue sections were cut using surgical knife and embedded in OCT blocks overnight at -80°C. The tendon tissue samples were cut at an arbitrary angle ϕ with respect to the longitudinal direction to artificially generate 3D structures [fig. 3.1]. Regions of porcine sclera near the optical nerve were cut in 35-μm-thick sections, with the Leica CM3050 cryostat (Leica Microsystems Inc., Buffalo Grove, IL, USA), since we expect colla-

gen fibers to be organized in various orientations in this region. Tissue slices were soaked in 1x PBS to remove excess OCT, and mounted onto glass slides using a permanent aqueous mounting media.

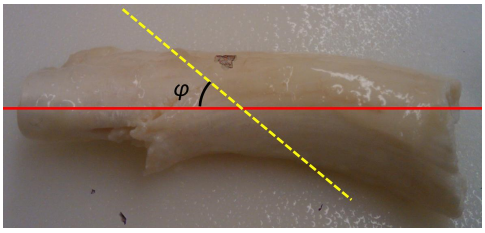

Figure 3.1: The porcine tendon tissue was cut along the yellow dashed line at an arbitrary angle ϕ with respect to the longitudinal axis (red line) [13].

3.2.2 Image Acquisition

Each image stack was acquired by using the Zeiss LSM 710 confocal microscope (Carl Zeiss Microscopy, Maple Grove, MN 55369, USA). The light source was a tunable Ti:Sapphire laser (Newport Corporation, Irvine, CA, USA) that produces 70 femtosecond-duration pulses spectrally centered at 780 nm at 80-MHz repetition rate. A half-wave plate was used to generate circularly polarized light to ensure SHG emission from collagen fibers at all orientations. A short-pass 760-nm dichroic beam splitter was placed inside the microscope to reflect the beam towards the sample. A 1.2 NA water immersion objective was used to focus the beam onto the sample. Backscattered SHG signal was collected through the same objective, and projected onto a non-descanned detector. In order to avoid uncertainty due to inter-

polation between consecutive images, each image stack was taken with an axial step size that is similar to the size of each pixel on the lateral plane. For sclera, the scanning step between images is 100 nm, and the x-y pixel size is 104 nm. For tendon, the z-step-size is 140 nm and the x-y pixel size is 139 nm.

3.2.3 Imaging Processing

The Canny edge detection algorithm was implemented for use in extracting surfaces of collagen fibers from 3D image stacks [58]. Canny's algorithm consists of the following four steps: 1. Smoothing, 2. Calculation of the intensity gradient, 3. Hysteresis thresholding, and 4. Non-maximum suppression [58]. In order to mitigate the effect of Poisson noise, each image stack is smoothed by using a 3D Gaussian filter [55, 58]. Since SHG signals are observed only at locations that contain collagen fibers, we can estimate locations of surfaces of collagen fibers by identifying areas with high intensity gradient values. In order to improve the continuity of surfaces, Canny's algorithm applies hysteresis thresholding [58]. Hysteresis thresholding utilizes two threshold values. The higher threshold value is used to choose voxels that are more likely to correspond to surfaces. The lower threshold value is then used to extend those surfaces by including less pronounced surfaces around them. Finally, non-maxima suppression was performed to limit the thickness of each surface to 1 voxel.

3.2.4 3D FT-SHG

Figure 3.2 demonstrates the procedures for calculating the local preferred orientation of collagen fibers in 3D space using 3D FT-SHG. With a 3D image stack obtained by using the aforementioned setup, a 3D grid was first created to divide the image stack into a set of smaller regions. The preferred orientation of collagen fibers within each smaller region was calculated using the filter bank method [59–61]. The filter bank consists of various 3D orientation filters constructed in the Fourier space. The 3D Fourier-transform of each region is then compared with the filter banks, and the filter that corresponds to the maximum correlation provides the best estimation of the preferred orientation. In order to decrease the computational time, we utilized the coarse to fine searching technique that we iteratively add filter banks around the coarse orientation to calculate the precise orientation [61]. If the average voxel intensity or the orientation anisotropy of a region is too low, calculation for the preferred orientation for such region becomes unnecessary [7,11,12]. A dark threshold determines the minimal average voxel intensity required for orientation analysis [7,11,12]. If the average voxel intensity of a region is lower than the dark threshold, the preferred orientation will not be calculated for that particular region. Since the coarse-to-fine approach was used for the orientation analysis, orientation anisotropy of each region was determined during the first iteration. If many orientation filters give a similar correlation value, there is no unique orientation, and the region is labeled as isotropic [7,11,12]. Consequently, the calculation for more precise results will not be carried out for that region.

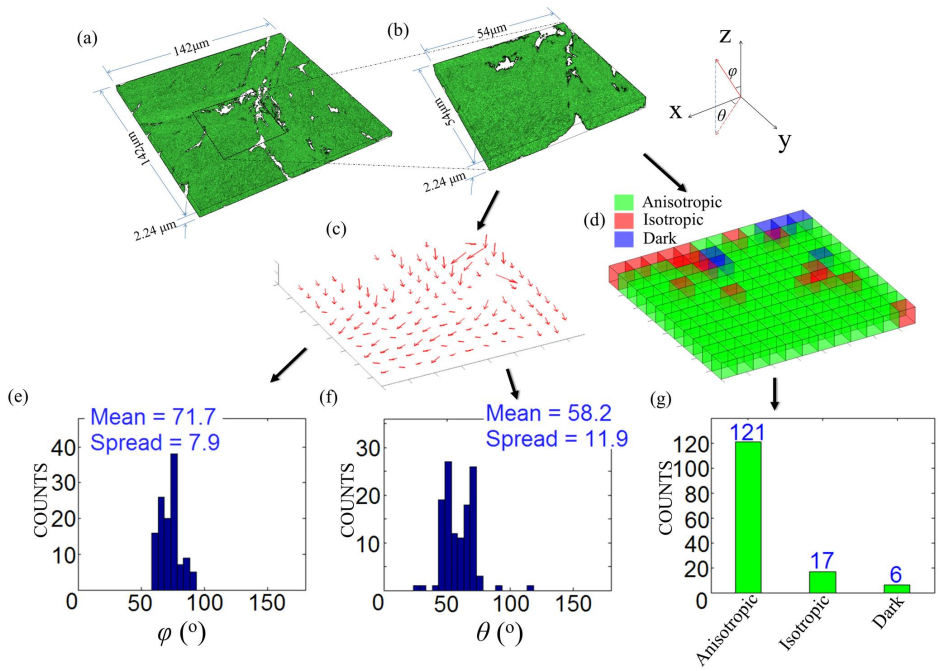

Figure 3.2: An illustration of applying 3D FT-SHG to quantifying arrangement of collagen fibers in 3D [13].

3.3 Results and discussion

3.3.1 Test Objects

Different test objects were generated to aid the evaluation of the accuracy and speed of our method. Figures 2a and 2b are examples of the cylindrical test objects (64 x 64 x 64) that were used for testing the accuracy of our method. According to the figures, the calculated orientation (red line) matches the test object (green cylinder) closely. The test objects were gen-

erated at 1° interval in both θ and ϕ directions of the spherical coordinate system from 0° through 360°. After a total number of 129,600 tests, we obtained a maximum error of 0.25° with a runtime of approximately 2.5 sec per test object. For a 256 x 256 x 96 test object with spirally curved surfaces shown in Fig. 3.3., the runtime was approximately 1.5 min on a desktop computer with a 3.4 GHz processor and 8 GB of RAM. Similar tests were performed on bigger test objects with sparse or dense features. In the case of a 512 x 512 x 512 sparse object with less than 15% of the total volume occupied, the runtime was approximately 5 min. Moreover, a dense object of the same size with more than 80% of total volume occupied took approximately 30 min.

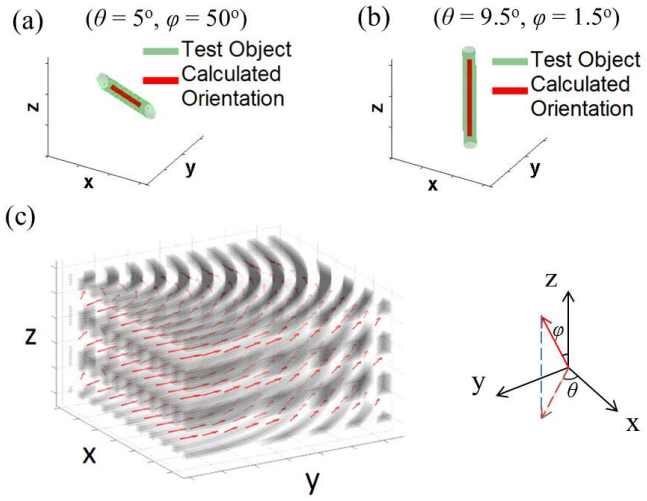

Figure 3.3: Cylindrical test objects (green) in 3D space and their calculated preferred orientation (red line) at (a) $\theta = 5.00°$, $\phi = 50.00°$, and (b) $\theta = 9.50°$, $\phi = 1.50°$. (c) A test object with a spiral pattern (gray) and the calculated local preferred orientations (red arrows) [13].

3.3.2 Porcine Sclera Tissue

3D FT-SHG analysis was performed on an image stack of a porcine sclera sample obtained from near the optic nerve [Fig. 3.4(a)]. A 3D model of the image stacks [Fig. 3.4(b)] was generated using an open-source 3D rendering software: Volview [62]. The analysis shows that collagen fibers in porcine sclera are primarily arranged in layers [Fig. 3.4(c)]. Moreover, the 3D quiver plot of the porcine sclera sample [Fig. 3.4(c)] closely resembles the 3D models [Fig. 3.4(b)]. The histogram of ϕ [Fig. 3.4(d)] shows a single peak centered at 87.5°. Such consistency in ϕ indicates that the porcine sclera consists of parallel sheets of collagen fibers. By observation, collagen

fibers are aligned along similar preferred orientations within each layer [Fig. 3.4(c)]. However, fiber orientations are different between different layers, which lead to multiple peaks on the orientation histogram in Fig. 3.4(e). A similar trend in collagen fiber distribution is also observed from Fig. 3.4(f) whereby collagen fibers are arranged in discrete layers in porcine sclera. Moreover, both the SHG image and the statistics of labeled regions show that a large portion of the tissue was not occupied by collagen fibers [Fig. 3.4(g)]; more than 50% of the total volume is labeled as dark regions [Fig. 3.4(g)].

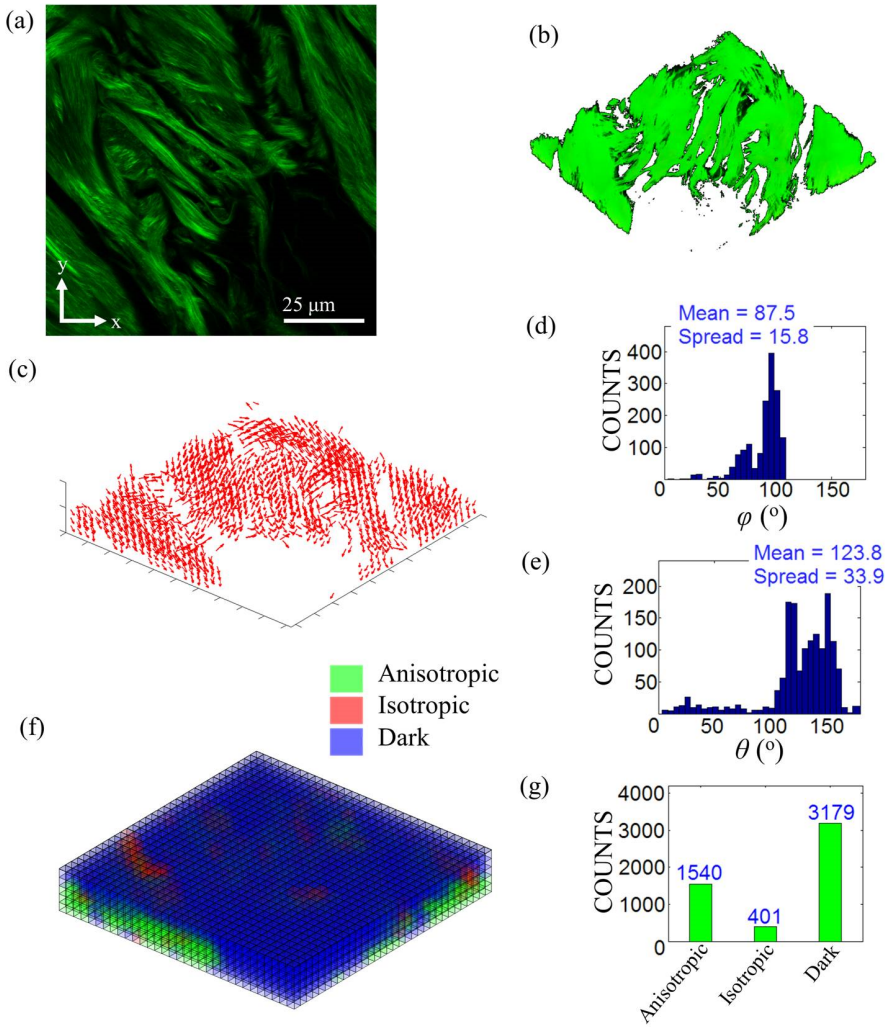

Figure 3.4: (a) A 102.4 μm x 102.4 μm x 16.2 μm image stack of porcine sclera tissue. (b) 3D model of the image stack. (c) 3D quiver plot that shows local fiber orientations of anisotropic regions. (d) Orientation histogram of collagen fibers with respect to the z-axis. (e) Orientation histogram of collagen fibers on the xy-plane. (f) 3D plot of labeled regions that shows location of anisotropic, isotropic, and dark regions. (g) Histogram of the numbers of labeled regions in the analyzed image [13].

3.3.3 Porcine tendon tissue

3D FT-SHG was used to analyze a porcine tendon sample that was sliced at an arbitrary angle [Fig. 3.5(a)]. Again, a 3D model of the image stacks [Fig. 3.5(b)] was generated using Volview. The Matlab generated 3D quiver plot [Fig. 3.5(c)] also resembles the shape of the 3D model. The calculated preferred orientations with respect to the z-axis, ϕ, are not centered at 90° [Fig. 3.5(d)]; rather, it indicates that there are collagen fibers oriented across the image stacks. The mean ϕ value of the tissue slice centers at 36.8° [Fig. 3.5(d)]. This may be indicative of the cut angle with respect to longitudinal axis (see Fig. 3.1). Moreover, our analysis shows that collagen fibers are aligned along similar preferred orientations within each fascicle as seen from Fig. 3.5(c). The histogram of θ displays a major peak value at 122.8° [Fig. 3.5(e)]; it supports the fact that collagen fibers are algined in similar orientation within each fascicle, as well as between different fascicles [9]. The analysis on the distribution of labeled regions reveals that porcine tendon tissues are dense fibrillar tissues [Fig. 3.5(f)] based on an insignificant number of dark regions [Fig. 3.5(g)].

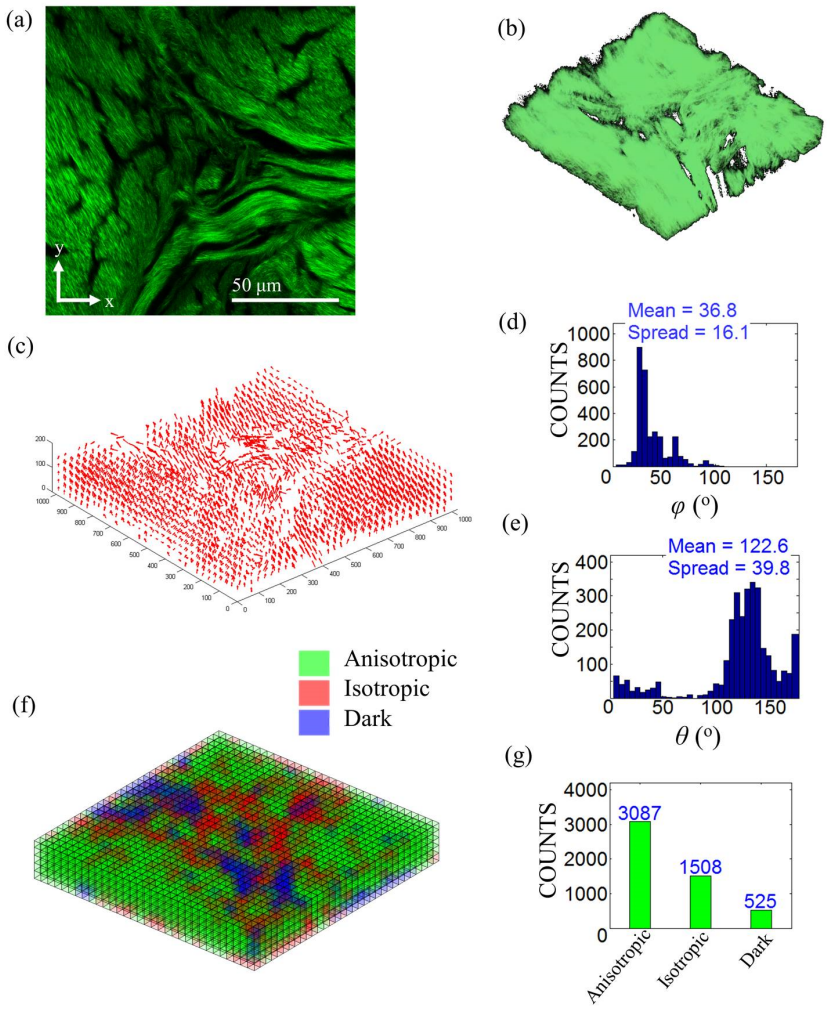

Figure 3.5: (a) A 142 μm x 142 μm x 21.5 μm image stack of porcine tendon tissue. (b) 3D model of the image stack. (c) 3D quiver plot that shows fiber orientations of anisotropic regions. (d) Orientation histogram of collagen fibers with respect to the z-axis (e) Orientation histogram of collagen fibers on the xy-plane. (f) 3D plot of labeled regions shows location of anisotropic, isotropic, and dark regions (g) A histogram of the numbers of labeled regions in the analyzed image [13].

3.3.4 2D FT-SHG versus 3D FT-SHG

Figure 3.6. is a comparative analysis of 2D FT-SHG and 3D FT-SHG as applied to porcine tendon sample sliced at an arbitrary angle. We observe, from both methods, similar trends of preferred fiber orientation [Figs. 3.6(a) and 3.6(b)]. In addition, relatively small spreads (spread = 15.8° for 2D FT-SHG and 6.4° for 3D FT-SHG) in the preferred orientation of collagen fibers are observed from Figs. 3.6(c) and 3.6(d). For the region highlighted in red, the 2D approach failed to compute fiber orientation that were not restricted to the transverse plane. Since collagen fibers are held together as bundles (fascicles) in tendon, they appear as individual disks on the cross-section image. In contrast, since the 3D analysis considers the entire image stack, disks on the cross-section images will stack up and form cylinders in 3D space. Therefore, the 3D method can resolve such uncertainty that occurs in 2D analysis. Similarly to the previous section, 3D FT-SHG shows that collagen fibers are oriented obliquely to the transverse plane as the histogram of ϕ was not centered at 90° [Fig. 3.6(e)]; it shows that the sample could be sliced at 67.9° with respect to the longitudinal direction (see Fig. 3.1). Similar population distributions of anisotropic, isotropic, and dark regions [Figs. 3.6(f) and 3.6(g)] are obtained from both methods. Consistent with our findings from the previous section, porcine tendon is a densely packed collagenous tissue that the number of dark regions is relatively negligible [Figs. 3.6(f) and 3.6(g)].

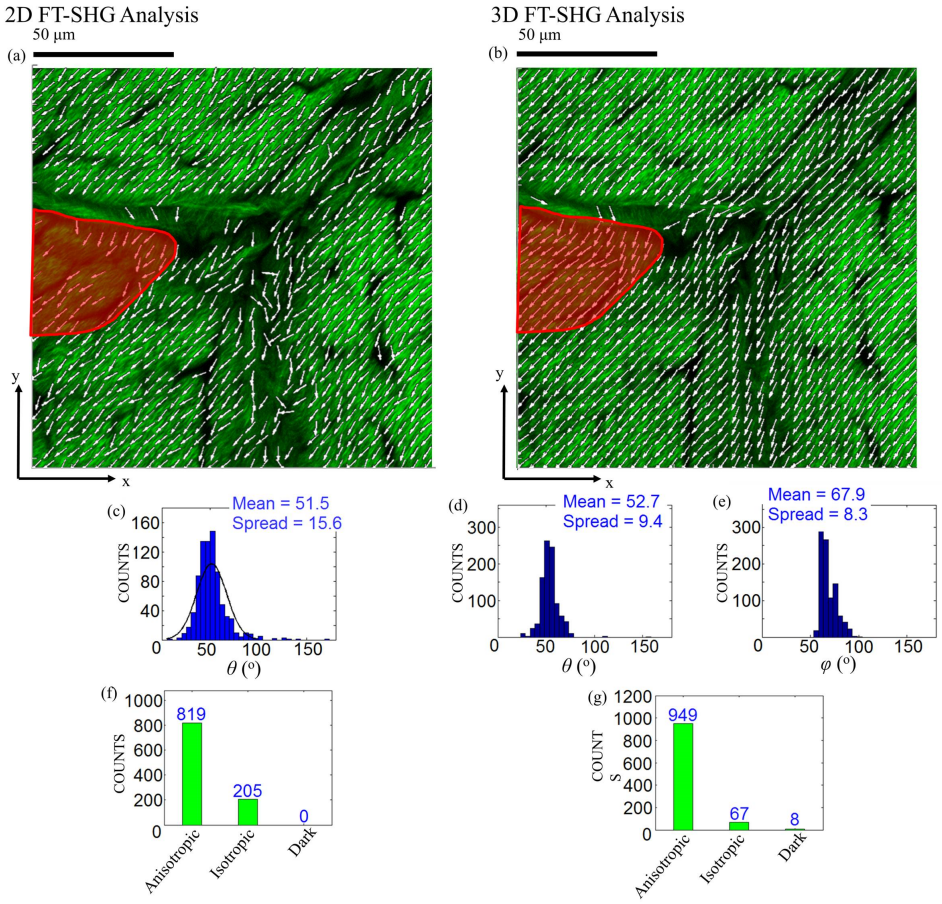

Figure 3.6: (a, b) Overlaid plots of the quiver plot of local preferred orientation and the SHG image of a porcine tendon sample. (c,d) Histograms of the in-plane orientation of collagen fibers. (e) Histogram of orientation of collagen fibers with respect to the z-axis obtained from the 3D analysis. (f, g) Histograms of labeled regions in the analyzed image [13].

3.4 Conclusion

3D FT-SHG applied 3D spatial Fourier analysis to quantify the spatial structure of collagen-based tissues in 3D. As an extension of 2D FT-SHG, 3D FT-SHG quantifies collagen-based tissues in 3D based on preferred orientations, orientation anisotropy, and average voxel intensity. The application of 3D FT-SHG on the computer generated test objects showed that 3D orientation can be solved accurately and relatively quickly by combining 3D spatial Fourier analysis and the coarse-to-fine searching technique. The example applications of 3D FT-SHG to porcine sclera and tendon demonstrated that 3D FT-SHG can effectively evaluate collagen fiber spatial organization in 3D. We believe that this technique is particularly useful for studying biological tissues that consist of 3D hierarchical structures made of collagen fibers [19, 35, 40, 56, 63].

Chapter 4

Application of FT-SHG to rat cervical tissues

4.1 Introduction

4.1.1 Background

Preterm birth is the condition that an infant is born prematurely before 37 weeks of gestation. Each year, there are 15 million preterm birth cases worldwide [64]. The incidence of infant mortality, debilitating morbidity and diseases (e.g. cardiovascular disease, hypertension, neurocognitive disorders, respiratory conditions, etc.) is more likely for premature infants [65,66]. Although much effort has been made in recent decades on improving caring for premature infants, there has been very little improvement on the prediction and prevention of preterm birth [67]. For instance, mainstream clinical interventions aimed at stopping preterm uterus contraction are ineffective to

reduce the incidence of preterm labor [68]. Therefore, an improved understanding of the cervical structure is needed for developing effective solutions to this problem.

4.1.2 Functions of the cervix during pregnancy

During the early stage of pregnancy, the cervix is firm in order to maintain pregnancy. Towards the end of gestation, it softens in order to allow the fetus to exit through the cervical canal [69–71]. This dramatic change in stiffness is due to cervical remodeling, a phase that causes significant alteration in the microstructure and composition of the cervix several months prior to labor [69,71]. During cervical remodeling, the cervix softens by disorganizing collagen structures and reducing collagen content [72–74]. The dense and firm fibrous structure in the cervix becomes soft and distensible. Imaging techniques, such as X-ray diffraction [75], polarized light microscopy [76], electron microscopy [76] and second-harmonic generation (SHG) microscopy [70, 77, 78] were used in previous studies to observe such morphological changes in cervical tissues due to cervical remodeling. However, many of the imaging techniques do not preserve the original microstructure because of exposure to ionizing radiation, or exogenous staining.

In this chapter, we are going to demonstrate the application of Fourier transform-second-harmonic generation (FT-SHG) imaging to quantify collagen fiber organization in the rat cervix. It is a quantitative imaging tech-

nique that uniquely combines SHG imaging with spatial Fourier analysis. It requires minimally invasive sample preparation because there is no need for exogenous staining. By applying spatial Fourier analysis to SHG images, it can quantify the morphology of the rat cervix with high specificity to collagen fibers. In section 2 of this chapter, we will describe our methodology, including sample preparation, image acquisition and analysis. In section 3, we will discuss the application of FT-SHG to quantify non-pregnant rat cervix. We will summarize this chapter in section 4.

4.2 Methods

4.2.1 Sample preparation

Rat cervical tissues were harvested from five non-pregnant rats using a protocol approved by the Institutional Animal Care and Use Committee at the University of Illinois at Urbana-Champaign. Harvested samples were embedded in OCT blocks and stored at -80°C until sectioning. For each embedded sample, 50-μm-thick transverse slices were obtained from proximal to the external orifice of the cervix (external os) and near the mid-cervix (half-way between the internal and external cervical os), as shown in Figure 4.1, using a Leica CM3050 cryostat (Leica Microsystems Inc., Buffalo Grove, IL, USA).

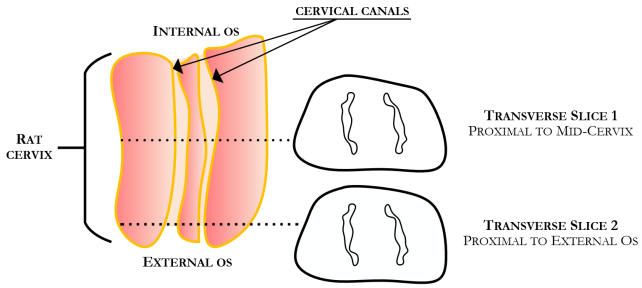

Figure 4.1: Schematic of the rat cervix. Transverse slices were taken from near the mid-cervix and the external orifice of the cervix (external os) [15].

4.2.2 Image acquisition

Epi-detected SHG images of cervical sections were acquired using a Zeiss LSM 710 confocal microscope (Carl Zeiss Microscopy, Maple Grove, MN 55369, USA) coupled with a femtosecond light source (Newport Corporation, Irvine, CA, USA) centered at 780-nm wavelength. The incident beam was circularly polarized to facilitate emission of SHG signals from collagen fibers at all orientations. In order to minimize spherical aberration due to refractive index mismatch between the sample and the imaging medium, a 1.2 numerical-aperture water immersion objective lens was chosen for both sample illumination and signal collection. The combination of a short-pass 760-nm filter followed by a 390/20-nm band-pass filter was placed between the objective and a GaAsP-NDD detector to extract the back-scattered SHG signal.

Lateral scanning step sizes ranging from 208 nm to 2.1 μm were adapted for imaging rat cervical tissues at different scales. For imaging whole transverse

slices of rat cervix, SHG images were acquired at a lateral step size of 2.1 μm. A lateral step size of 208 nm was used to obtain higher resolution images of the selected characteristic regions. 3D image stacks of the characteristic regions were obtained by taking consecutive images at a lateral step size of 208 nm and an axial step of 210 nm. Using similar step sizes in both lateral and axial directions can avoid interpolating between consecutive images as interpolation may introduce uncertainties. Among the five rat cervices used in this study, three were used for 2D analysis and two were used for 3D analysis. A complete image of each transverse slice was taken for all rat cervices.

4.2.3 Image analysis

To quantitatively assess the arrangement of collagen fibers in the rat cervix, FT-SHG was applied in both 2D and 3D. Briefly, Fourier transform (FT) analysis was performed on gridded (2D) SHG images as well as (3D) image stacks; each region bounded by the grid was examined individually. The grid size was carefully chosen such that each bounded region was small enough to describe the local orientation of collagen fibers while avoiding errors due to pixelation. Each region that displayed a dominant orientation in the frequency spectrum was labeled as anisotropic and assigned a preferred orientation, whereas regions that lacked prominent orientations were labeled as isotropic. In addition, regions with low or negligible SHG intensity did not provide representative information of orientation isotropy; those regions were consequently labeled as dark regions. In this chapter, we have utilized the circular variance as the metric for quantifying orientation isotropy of

SHG images. The circular variance is a dimensionless measurement of the spread of orientation [79, 80], and has a value between 0 and 1; the smaller the circular variance, the smaller the spread of preferred orientation.

4.3 Results and discussion

4.3.1 2D FT-SHG

Figure 4.2(a) is a representative image of a tissue slice obtained from the mid-cervix. The FT analysis shows a loop of highly aligned collagen fibers that is symmetric about both the sagittal and coronal planes. Areas adjacent to the highly aligned fibers and between the cervical canals are predominantly isotropic [Fig. 4.2(b)]. For a tissue slice obtained from near the external os of the same rat cervix, the analysis displays similar arrangement of collagen fibers [Figs. 4.2(c) and 4.2(d)]. Likewise, tissue slices from four additional rat cervix samples contain similar spatial arrangement of collagen fibers at both locations. This initial evaluation of the rat cervix indicates symmetries and consistency in fiber organization on the transverse plane and along the longitudinal direction of the organ, respectively. Therefore, it allows us to select representative characteristic regions for a more detailed evaluation of collagen fiber organization.

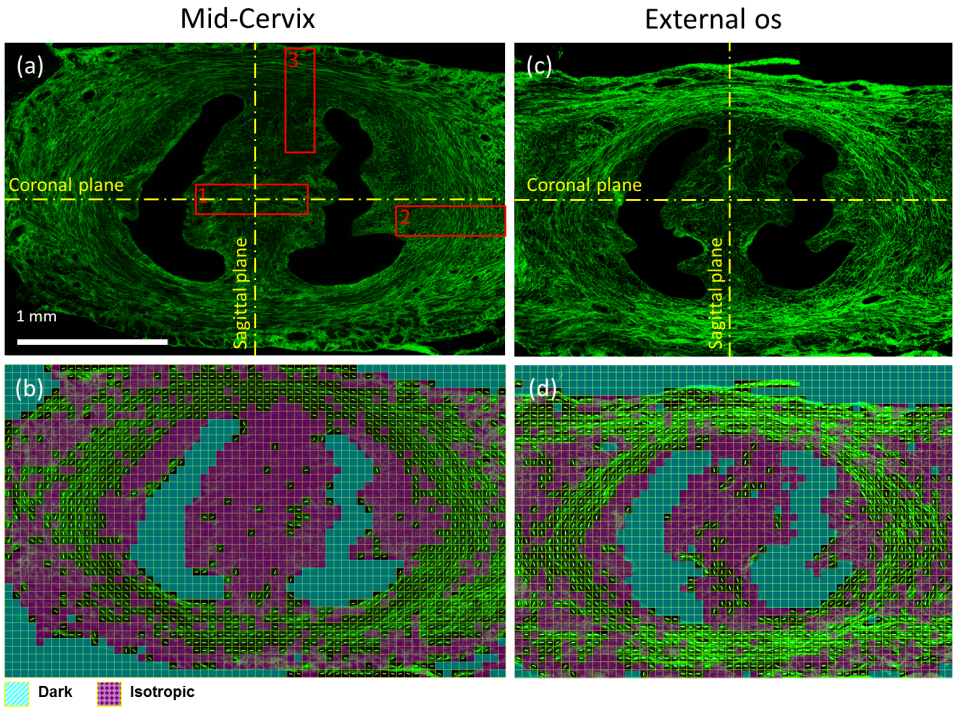

Figure 4.2: 2. (a) An SHG image of a tissue section from the mid-cervix. The characteristic regions are highlighted by the red boxes. (b) Results of FT-SHG analysis of (a). (c),(d) The SHG image and results of FT-SHG analysis of a tissue section near the external os of the same cervix sample. The scale is the same for (a-d) and the scale bar is shown in (a) [15].

Three characteristic regions from both the mid-cervix and external os were selected and analyzed at higher resolution with a lateral step size of 208 nm (number of animals, n = 3) [Fig. 4.3]. The circular histograms of preferred orientation of anisotropic regions are shown alongside their corresponding SHG images in Fig. 4.3. Averaging over the six tissue slices analyzed, the circular variances of the region between the cervical canals, and the two re-

gions showing predominately circumferentially-oriented fibers near the coronal plane and the sagittal plane are 0.187, 0.132, and 0.0898, respectively. In the same order, the ratio of the number of anisotropic regions to the number of isotropic regions are 1.40 (standard deviation = 1.27), 1.87 (standard deviation = 0.614), and 1.61 (standard deviation = 0.297).

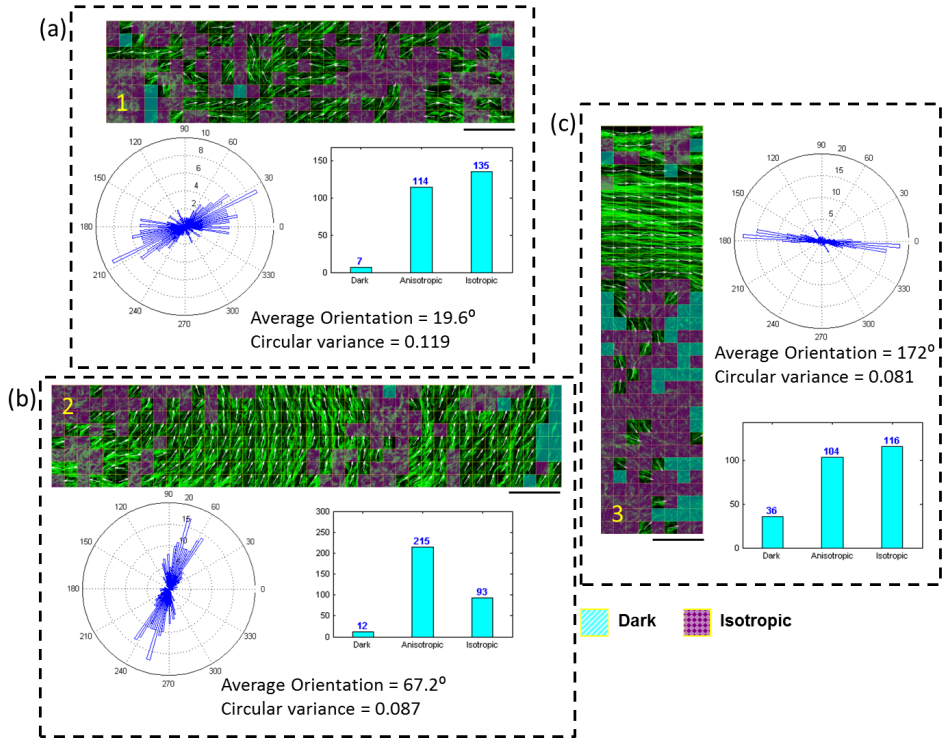

Figure 4.3: Results of FT-SHG of the characteristic regions indicated on Fig. 4.2(a). (a) The SHG image of the region between the cervical canals and near the intersection of the sagittal and coronal planes. It is overlaid with colored blocks indicating spatial locations of the labeled regions. White arrows represents preferred orientations of anisotropic regions. A circular histogram summarizing the distribution of preferred orientation of the anisotropic regions and a histogram of labeled regions are generated for quantitative evaluation and comparison between different characteristic regions. The same analysis is shown for region 2 and region 3 labeled on Fig. 4.2(a), in (b) and (c), respectively. The coronal plane and the sagittal plane correspond to 0° and 90° on the circular histograms. Scale bar = 100 μm [15].

The region between the cervical canals, proximal to the intersection of the sagittal and coronal planes (region 1), has a higher circular variance relative to the regions that contain the circumferentially oriented fibers. The higher circular variance indicates that the organization of collagen fibers in this region is more isotropic, i.e., the collagen fibers are less aligned. In fact, the SHG image of the central region displays an interwoven network of collagen fibers in many different orientations [Fig. 4.2(a)]. Consistently, the FT-SHG analysis shows that isotropic regions and anisotropic regions are randomly distributed across the central region [Fig. 4.3(a)]. For the regions that contain circumferentially oriented fibers, their circular histograms display relatively low circular variances, which indicate that collagen fibers along the circumferential loop are highly aligned. Similar to Figure 4.2(a), areas in the immediate surroundings of the highly aligned fibers are relatively isotropic for both regions. Therefore, regions 2 and 3 are approximately equivalent to each other.

4.3.2 3D FT-SHG

Based on the aforementioned analysis, the rat cervix can be divides into three distinct sections according to the fiber arrangement: a section with highly aligned collagen fibers sandwiched between two isotropic sections [Fig. 4.4]. In addition, the isotropic sections also point to a potential 3D fibrillar structure present in the rat cervix. The previous chapter has indicated that isotropic regions indicated by the 2D FT analysis may contain out-of-plane fibers with respect to the image plane due to the fact that each 2D image can only capture a small portion of their lengths (Lau et al., 2012). In

comparison, 3D FT-SHG analyze multiple images throughout the depth of the tissue, and therefore avoids such ambiguity. As a result, 3D FT-SHG may provide a more comprehensive evaluation of the morphology of the rat cervix.

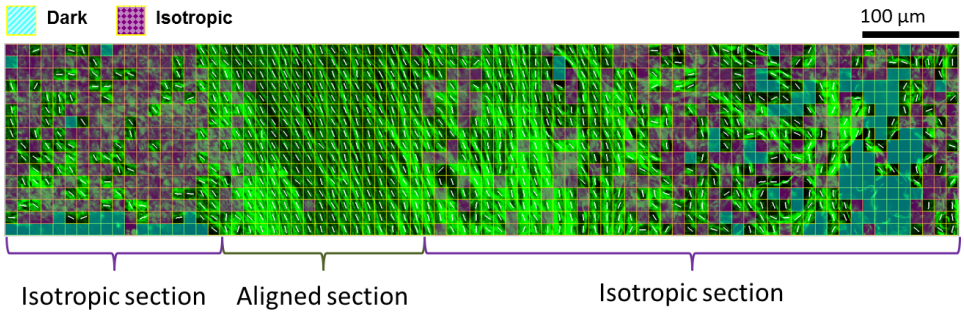

Figure 4.4: A representative illustration of the three sections of the region outside of the cervical canals (indicated as region 2 on Fig. 4.2(a)). Each section has a distinct spatial arrangement. As part of the loop of aligned fibers mentioned in the initial evaluation, the section sandwiched between two isotropic sections contains highly organized collagen fibers. Sections adjacent to that are predominantly isotropic. According the SHG image, the isotropic sections consist of randomly distributed isotropic and anisotropic regions [15].

Figure 4.5 displays results of the 2D and 3D FT-SHG analysis of a tissue section obtained from the mid-cervix. The 2D analysis of the SHG image of the tissue slice displays the same pattern of fiber arrangement as that in fig. 4.5(b). Two characteristic regions were chosen and analyzed from a 3D perspective. Despite the high orientation isotropy shown on the 2D image of the region, there is a significant number of out-of-plane collagen fibers between the canals according to the 3D rendered images as well as the 3D

FT-SHG analysis [Figs. 4.5(c) and (d)]. For the region outside of the cervical canals, labeled as region 2 in Fig. 4.5(a), there are a substantial number of out-of-plane fibers at locations that were identified as isotropic by the 2D analysis [Figs. 4.5(e) and (f)]. Similar arrangement of collagen fibers is also found in another sample of rat cervix. Therefore, the 3D analysis provides more revealing information of the fiber orientation in the areas that appear to be predominately isotropic on a 2D image.

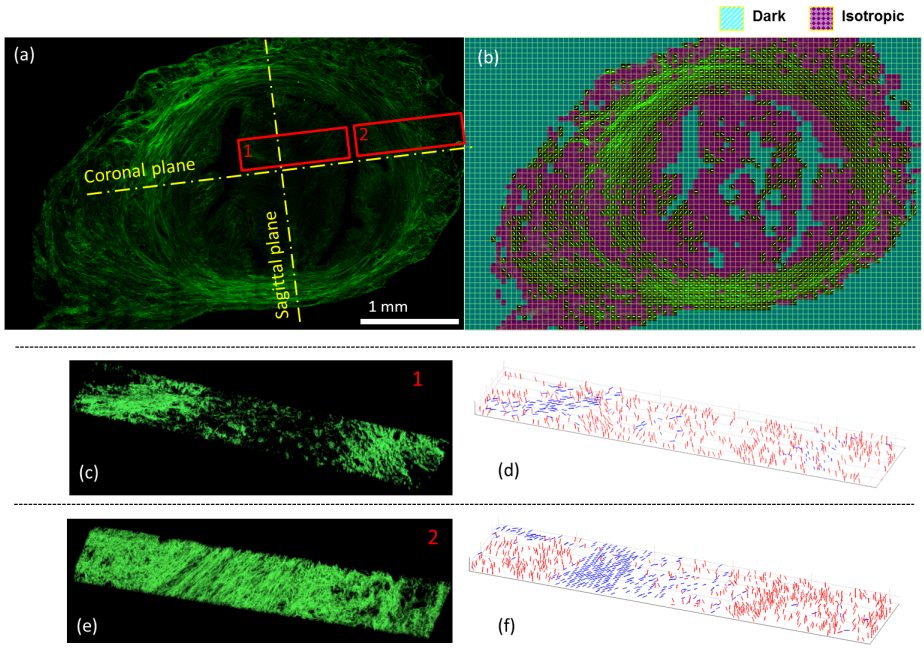

Figure 4.5: (a) The SHG image and (b) the 2D FT analysis of the transverse section show a group of highly aligned circumferential fibers. In addition, regions next to the highly aligned area and those between the cervical canals are mostly isotropic. Two characteristic regions chosen from the region between the cervical canals and the aligned region were imaged in 3D. For the region between the cervical canals, (c) the 3D rendered model, measuring 1062.5 μm x 212.5 μm x 23.5 μm and (d) the 3D FT analysis indicate the presence of a 3D fibrillar network. According to (e) the 3D rendered model of the outside region, measuring 1062.5 μm x 212.5 μm x 23.5 μm, and (f) its 3D FT analysis, out-of-plane fibers are also observed from those regions adjacent to the highly aligned regions. The blue arrows and red arrows indicate in-plane and out-of-plane orientations, respectively. The scale is the same for (a) and (b) and indicated in (a) [15].

As indicated by the 3D analysis in Fig. 4.6, there are out-of-plane fibers at some of the isotropic regions. Such findings are consistent with the rat cervix model from previous studies. It has been formerly established that there exists three concentric layers around each cervical canal in the rat cervix: a layer of circumferentially and transversely aligned fibers between two layers composed of predominately longitudinal fibers [76]. This spatial arrangement gives the rat cervix the desired shape and mechanical properties. Similar spatial arrangement is also found in the human cervix with the exception that there is only one cervical canal in the human cervix [73]. However, the similar characteristics between rat and human cervices indicate our technique can be potentially be applied to assess human cervical tissues.

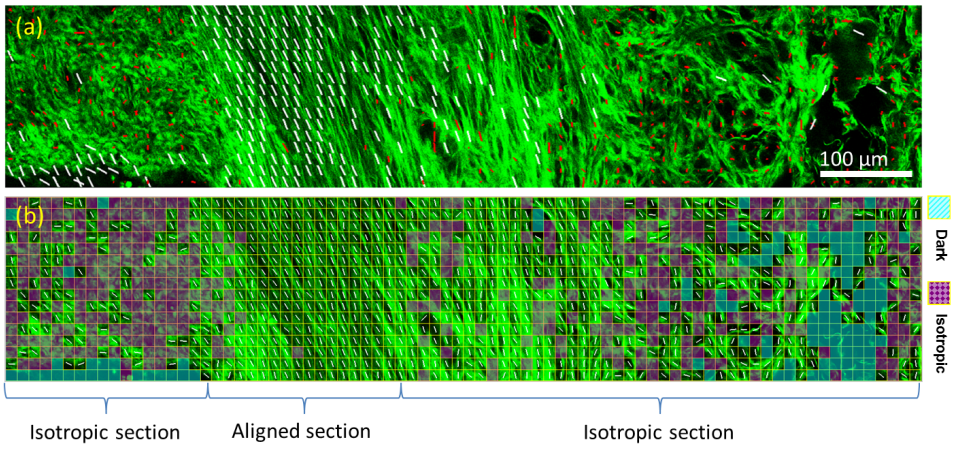

Figure 4.6: A comparison between (a) 3D FT-SHG and (b) 2D FT-SHG on a region outside of the cervical canals. For the 3D analysis, white lines and red lines in (a) represents in-plane and out-of-plane preferred orientations, respectively. At the isotropic sections previously identified using the 2D analysis, there exists a significant amount of out-of-plane fibers. The scale is the same for (a) and (b) and indicated in (a) [15].

4.4 Conclusion

Using FT-SHG, we have evaluated SHG images of unstained rat cervices from both 2D and 3D perspectives. The FT-SHG analysis of the rat cervix shows that the arrangement of collagen fibers varies as a function of location on the transverse plane, but maintains consistent along the longitudinal direction. Both 2D and 3D analysis highlights a loop of circumferentially aligned fibers in the rat cervix. However, only the 3D analysis is able to indicate that collagen fibers are predominantly aligned out-of-plane at the

immediate surroundings of this area and at the regions between the cervical canals. Based on the similarity between the structure of the rat cervix and that of the human cervix model proposed by previous studies, 3D FT-SHG has potential to be applied to the human cervix. Alongside the recent development of a fiber-optic SHG scanning endomicroscope by Zhang et al. [78], 3D FT-SHG can be a potential tool for minimally invasive assessment of premature cervical remodeling in humans.

Chapter 5

Conclusion

This thesis has reported the generalization of FT-SHG to quantify collagen-based biological tissues in 3D. By utilizing the 3D imaging capability of SHG microscopy and combining that with 3D spatial Fourier analysis, we can effectively evaluate the overall morphology of collagen-based tissues in a quantitative manner. As an extension of our previous technique, 3D FT-SHG quantifies tissues based on local preferred orientation, orientation isotropy, and average SHG intensity. Although 3D analysis involves extensive manipulation of large data set, we utilized the filter-bank technique and coarse-to-fine searching in our algorithm to minimize the number of iterations and maximize the efficiency of our technique. By the use of a large number of computer generated test objects, we have validated that our technique can calculate 3D preferred orientation efficiently and accurately.

The example applications to porcine sclera and porcine tendon have demon-

strated the utility of 3D FT-SHG to quantify biological tissues. The consistency between the original SHG images and the results obtained from 3D FT-SHG indicates the promising potential of applying 3D FT-SHG to solve real biological problems. Therefore, our recent study has applied 3D FT-SHG to quantify rat cervical tissues. Previous studies have formerly stated that preterm birth is associated with early cervical remodeling, a process that disorganizes collagen microstructures and reduces collagen content in the cervix. Therefore, an imaging technique that can accurately assess changes in the microstructures of the cervix will be an invaluable resource for the development of effective solutions to preterm birth. Based on our recent study, spatial information of the rat cervix can be extracted readily from both 2D and 3D perspectives using FT-SHG. Our results has not only restated the promising utility of FT-SHG, but also proposed an effective technique for accessing morphological changes in cervical tissues. It could be a potential tool for detecting the likelihood of preterm birth.

In the immediate future, the development of simultaneous SHG imaging and analysis will be essential for developing our technique for medical applications. By integrating our existing FT-SHG graphical-user-interface application with a microscope system, both imaging and analysis can be performed at the same time. Alongside improvements in imaging systems and developments of more efficient algorithms, FT-SHG can potentially be applied to real-time, *in vivo* applications.

References

[1] B. Alberts, A. Johnson, L. Julian, R. Martin, R. Keith, and W. Peter, *Molecular Biology of the Cell* (Garland Science, 2007), 5th ed.

[2] P. Fratzl, *Collagen: Structure and Mechanics* (Springer, 2008), 1st ed.

[3] M. Sivaguru, S. Durgam, R. Ambekar, D. Luedtke, G. Fried, A. Stewart, and K. C. Toussaint, "Quantitative analysis of collagen fiber organization in injured tendons using Fourier transform-second harmonic generation imaging," Opt. Express **18**, 24983–24993 (2010).

[4] R. Ambekar, T.-Y. Lau, M. Walsh, R. Bhargava, and K. C. Toussaint, "Quantifying collagen structure in breast biopsies using second-harmonic generation imaging," Biomed. Opt. Express **3**, 2021–2035 (2012).

[5] O. Nadiarnykh, R. LaComb, M. Brewer, and P. J. Campagnola, "Alterations of the extracellular matrix in ovarian cancer studied by second harmonic generation imaging microscopy," BMC Cancer **10**, 94 (2010).

[6] T. Hompland, A. Erikson, M. Lindgren, T. Lindmo, and C. L. Davies, "Second-harmonic generation in collagen as a potential cancer diagnostic parameter," J. Biomed. Opt. **13**, 54011–54050 (2008).

[7] P. J. Campagnola, M. A. Brewer, V. Ajeti, P. Keely, K. Eliceiri, M. Patankar, and K. Tilbury, "SHG imaging of cancer," in "Biomedical Optics," (Optical Society of America, 2012), p. BSu4B.1.

[8] D. Barkan, J. E. Green, and A. F. Chambers, "Extracellular matrix: a gatekeeper in the transition from dormancy to metastatic growth," Eur. J. Cancer **46**, 1181–1188 (2010).

[9] N. Maffulli, P. Renstrom, and W. B. Leadbetter, *Tendon Injuries: Basic Science and Clinical Medicine* (Springer, 2005), 1st ed.

[10] R. Ambekar Ramachandra Rao, M. R. Mehta, S. Leithem, and K. C. Toussaint, "Quantitative analysis of forward and backward second-harmonic images of collagen fibers using Fourier transform second-harmonic-generation microscopy," Opt. Lett. **34**, 3779–3781 (2009).

[11] R. Ambekar, M. R. Mehta, S. Leithem, and K. C. Toussaint, "Fourier transform-second-harmonic generation imaging of collagen fibers in biological tissues," in "Biomedical Optics," (Optical Society of America, 2010), p. BSuD63.

[12] R. Ambekar, M. Chittenden, I. Jasiuk, and K. C. Toussaint, "Quantitative second-harmonic generation microscopy for imaging porcine cortical bone: comparison to SEM and its potential to investigate age-related changes," Bone **50**, 643–650 (2011).

[13] T. Y. Lau, R. Ambekar, and K. C. Toussaint, "Quantification of collagen fiber organization using three-dimensional Fourier transform-second-harmonic generation imaging," Opt. Express **20**, 21821–21832 (2012).

[14] T. Y. Lau, R. Ambekar, and K. C. Toussaint, "Three-Dimensional Fourier-Transform Second-Harmonic Generation Microscopy for Quantification of Collagen Fiber Organization in Biological Tissues," in "Frontiers in Optics Conference," (Optical Society of America, 2012), OSA Technical Digest (online), p. FM3D.7.

[15] T. Y. Lau, H. K. Sangha, E. K. Chien, B. L. McFarlin, A. J. Wagoner-Johnson, and K. C. Toussaint, "Application of Fourier transform-second-harmonic generation imaging to the rat cervix," Journal of Microscopy (2013, in press).

[16] R. Ambekar and K. C. Toussaint, "Investigation of Collagen Fiber Organization in Cornea and Sclera using Quantitative SHG Microscopy," in "Frontiers in Optics," (Optical Society of America, 2011), OSA Technical Digest, p. FTuQ2.

[17] R. Ambekar, K. C. Toussaint, and A. W. Johnson, "The effect of keratoconus on the structural, mechanical, and optical properties of the cornea," J. Mech. Behav. Biomed. Mat. **4**, 223–236 (2010).

[18] M. Fatima-Vaz, H. Canhao, and F. Joao-Eurico, *Bone: A Composite Natural Material* (InTech, 2011).

[19] M. F. Young, "Bone matrix proteins: their function, regulation, and relationship to osteoporosis," Osteo. Int. **14**, 35–42 (2003).

[20] R. Ambekar, "Quantification of Collagen Fiber Organization in Biological Tissues at Cellular and Molecular Scales Using Second-Harmonic Generation Imaging," Ph.D. thesis, University of Illinois at Urbana-Champaign (2012).

[21] T. Abraham, D. Kayra, B. McManus, and A. Scott, "Quantitative assessment of forward and backward second harmonic three dimensional images of collagen type I matrix remodeling in a stimulated cellular environment," J. Struc. Biol. (2012).

[22] J. Caetano-Lopes, A. Nery, H. Canhao, J. D. R. Cascao, A. Rodrigues, I. Perpetuo, S. Abdulghani, P. Amaral, S. Sakaguchi, Y. Konttinen, L. Graca, M. Vaz, and J. Fonseca, "Chronic arthritis leads to disturbances in the bone collagen network," Arth. Res. Thera. **12**, R9 (2010).

[23] N. Morishige, N. Yamada, S. Teranishi, T.-i. Chikama, T. Nishida, and A. Takahara, "Detection of subepithelial fibrosis associated with corneal stromal edema by second harmonic generation imaging microscopy," Invest. Ophth. Vis. Sci. **50**, 3145–3150 (2009).

[24] P. Stoller, B.-M. Kim, A. M. Rubenchik, K. M. Reiser, and L. B. Da Silva, "Polarization-dependent optical second-harmonic imaging of a rat-tail tendon," Journal of Biomedical Optics **7**, 205–214 (2002).

[25] P. J. Su, W. L. Chen, T. H. Li, C. K. Chou, T. H. Chen, Y. Y. Ho, C. H. Huang, S. J. Chang, Y. Y. Huang, H. S. Lee, and C. Y. Dong, "The discrimination of type I and type II collagen and the label-free imaging of engineered cartilage tissue," Biomaterials **31**, 9415–9421 (2010).

[26] C. P. Brown, M. A. Houle, M. Chen, A. J. Price, F. Légaré, and H. S. Gill, "Damage initiation and progression in the cartilage surface probed by nonlinear optical microscopy," J. Mech. Behavior Biomed. Mat. **5**, 62–70 (2012).

[27] E. Werkmeister, N. D. Isla, P. Netter, J. Stoltz, and D. Dumas, "Collagenous extracellular matrix of cartilage submitted to mechanical forces studied by second harmonic generation microscopy," Photochem. Photobiol. **86**, 302–310 (2009).

[28] P. J. Campagnola and L. M. Loew, "Second-harmonic imaging microscopy for visualizing biomolecular arrays in cells, tissues and organisms," Nat. Biotech. **21**, 1356–1360 (2003).

[29] R. A. Rao, M. R. Mehta, and K. C. Toussaint, "Fourier transform-second-harmonic generation imaging of biological tissues," Opt. Express **17**, 14534–14542 (2009).

[30] M. J. Silva, M. D. Brodt, B. Wopenka, S. Thomopoulos, D. Williams, M. H. M. Wassen, M. Ko, N. Kusano, and R. A. Bank, "Decreased collagen organization and content are associated with reduced strength of demineralized and intact bone in the SAMP6 mouse," J. Bone Min. Res. **21**, 78–88 (2006).

[31] S. M. Weis, J. L. Emery, K. D. Becker, D. J. McBride, J. H. Omens, and A. D. McCulloch, "Myocardial mechanics and collagen structure in the osteogenesis imperfecta murine (oim)," Circ. Res. **87**, 663–669 (2000).

[32] P. J. Campagnola, A. C. Millard, M. Terasaki, P. E. Hoppe, C. J. Malone, and W. A. Mohler, "Three-Dimensional High-Resolution Second-Harmonic Generation Imaging of Endogenous Structural Proteins in Biological Tissues," Biophysical Journal **82**, 493–508 (2002).

[33] C. Thrasivoulou, G. Virich, T. Krenacs, I. Korom, and D. L. Becker, "Optical delineation of human malignant melanoma using second harmonic imaging of collagen," Biomed. Opt. Express **2**, 1282–1295 (2011).

[34] D. F. Holmes, C. J. Gilpin, C. Baldock, U. Ziese, A. J. Koster, and K. E. Kadler, "Corneal collagen fibril structure in three dimensions: structural insights into fibril assembly, mechanical properties, and tissue organization," PNAS **98**, 7307–7312 (2001).

[35] S. Viguet-Carrin, P. Garnero, and P. Delmas, "The role of collagen in bone strength," Osteo. Int. **17**, 319–336 (2006).

[36] K. Brockbank, W. MacLellan, J. Xie, S. Hamm-Alvarez, Z. Chen, and K. Schenke-Layland, "Quantitative second harmonic generation imaging of cartilage damage," Cell Tis. Bank. **9**, 299–307 (2008).

[37] N. Morishige, Y. Takagi, T. Chikama, A. Takahara, and T. Nishida, "Three-dimensional analysis of collagen lamellae in the anterior stroma of the human cornea visualized by second harmonic generation imaging microscopy," Invest. Ophth. Vis. Sci. **52**, 911–915 (2007).

[38] C. Boote, S. Dennis, Y. Huang, A. J. Quantock, and K. M. Meek, "Lamellar orientation in human cornea in relation to mechanical properties," J. Struc. Biol. **149**, 1–6 (2005).

[39] Y. Komai and T. Ushiki, "The three-dimensional organization of collagen fibrils in the human cornea and sclera," Invest. phtha. Vis. Sci. **32**, 2244–2258 (1991).

[40] M. Winkler, D. Chai, S. Kriling, C. J. Nien, D. J. Brown, B. Jester, T. Juhasz, and J. V. Jester, "Nonlinear optical macroscopic assessment of 3-D corneal collagen organization and axial biomechanics," Invest. Ophth. Vis. Sci. **52**, 8818–8827 (2011).

[41] X. Chen, O. Nadiarynkh, S. Plotnikov, and P. J. Campagnola, "Second harmonic generation microscopy for quantitative analysis of collagen fibrillar structure," Nat. Protocols **7**, 654–669 (2012).

[42] B. Pourdeyhimi and H. S. Kim, "Measuring fiber orientation in nonwovens: the hough transform," Text. Res. J. **72**, 803–809 (2002).

[43] A. A. A. Jaddi, H. S. Kim, and B. Pourdeyhimi, "Measurement of fiber orientation in nonwovens optical fourier transform," Inter. Nonwovens J. **10**, 10–16 (2001).

[44] B. Josso, D. R. Burton, and M. J. Lalor, "Texture orientation and anisotropy calculation by Fourier transform and principal component analysis," Mech. Sys. Sig. Proc. **19**, 1152–1161 (2005).

[45] F. XiaoGuang and P. Milanfar, "Multiscale principal components analysis for image local orientation estimation," in "Signals, Systems and Computers, 2002. Conference Record of the Thirty-Sixth Asilomar Conference on," , vol. 1 (2002), vol. 1, pp. 478–482 vol.1.

[46] W. Yi and S. Marshall, "Principal component analysis in application to object orientation," Geo-Spat. Info. Sci. **3**, 76–78 (2000).

[47] S. Mori and P. C. M. van Zijl, "Fiber tracking: principles and strategies - a technical review," NMR Biomed. **15**, 468–480 (2002).

[48] N. Toussaint, M. Sermesant, C. T. Stoeck, S. Kozerke, and P. G. Batchelor, "In vivo human 3D cardiac fibre architecture: reconstruction using curvilinear interpolation of diffusion tensor images," Med. Imag. Comput. Assist. Interv. **13**, 418–425 (2010).

[49] J. Wu, B. Rajwa, D. L. Filmer, C. M. Hoffmann, B. Yuan, C. Chiang, J. Sturgis, and J. P. Robinson, "Analysis of orientations of collagen fibers by novel fiber-tracking software," Microscopy Microanal. **9**, 574–580 (2003).

[50] C. C. V. Donkelaar, L. J. G. Kretzers, P. H. M. Bovendeerd, L. M. A. Lataster, K. Nicolay, J. D. Janssen, and M. R. Drost, "Diffusion tensor imaging in biomechanical studies of skeletal muscle function," J. Anat. **194**, 79–88 (1999).

[51] O. Friman, G. Farneback, and C. F. Westin, "A Bayesian approach for stochastic white matter tractography," IEEE Trans. Med. Imag. **25**, 965–978 (2006).

[52] C. S. Garbe, A. Buttgereit, S. Schurmann, and O. Friedrich, "Automated multiscale morphometry of muscle disease from second harmonic generation microscopy using tensor-based image processing," IEEE Trans. Biomed. Engr. **59**, 39–44.

[53] P. Helm, M. F. Beg, M. I. Miller, and R. L. .Winslow, "Measuring and mapping cardiac fiber and laminar architecture using diffusion tensor MR imaging," Ann. NY Acad. Sci. **1047**, 296–307 (2005).

[54] H. Park, M. Kubicki, C. Westin, I. Talos, A. Brun, S. Peiper, R. Kikinis, F. A. Jolesz, R. W. McCarley, and M. E. Shenton, "Method for combining information from white matter fiber tracking and gray matter parcellation," Amer. J. Neuroradiol. **25**, 1318–1324 (2004).

[55] J. Wu, S. L. Voytik-Harbin, D. L. Filmer, C. M. Hoffman, B. Yuan, C.-S. Chiang, J. Sturgis, and J. P. Robinson, "Modeling ECM fiber formation: structure information extracted by analysis of 2D and 3D image sets," in "Three-Dimensional and Multidimensional Microscopy: Image Acquisition and Processing IX," , vol. 4621 (SPIE, San Jose, CA, USA, 2002), vol. 4621, pp. 52–56.

[56] A.-M. Pena, A. Fabre, D. Débarre, J. Marchal-Somme, B. Crestani, J.-L. Martin, E. Beaurepaire, and M.-C. Schanne-Klein, "Three-dimensional investigation and scoring of extracellular matrix remodeling during lung fibrosis using multiphoton microscopy," Microscopy Research and Technique **70**, 162–170 (2007).

[57] T. Sun, Y. Liu, M. Sung, H. Chen, C. Yang, V. Hovhannisyan, W. Lin, Y. Jeng, W. Chen, L. Chiou, G. Huang, K. Kim, P. T. C. So, Y. Chen,

H. Lee, and C. Dong, "Ex vivo imaging and quantification of liver fibrosis using second-harmonic generation microscopy," J. Biomed. Opt. **15**, 36002–36006 (2010).

[58] J. Canny, "A computational approach to edge detection," IEEE Trans. Pattern Anal. Mach. Intell. **PAMI-8**, 679–698 (1986).

[59] R. H. Bamberger and M. J. T. Smith, "A filter bank for the directional decomposition of images: theory and design," IEEE Trans. Sig. Proc. **40**, 882–893 (1992).

[60] A. K. Jain, S. Prabhakar, L. Hong, and S. Pankanti, "Filterbank-based fingerprint matching," IEEE Trans. Imag. Proc. **9**, 846–859 (2000).

[61] D. A. Forsyth and J. Ponce, *Computer Vision: A modern approach* (Prentice Hall, 2011).

[62] Kitware, "Volview," .

[63] T. Abraham and J. Hogg, "Extracellular matrix remodeling of lung alveolar walls in three dimensional space identified using second harmonic generation and multiphoton excitation fluorescence," J. Struc. Biol. **171**, 189–196 (2010).

[64] March of Dimes, PMNCH, Save the Children, and World Health Organization, "Born Too Soon: The Global Action Report on Preterm Birth," Tech. rep., World Health Organization, Geneva (2012).

[65] March of Dimes, "Data Book for Policy Makers: Maternal, Infant, and Child Health in the United States," Tech. rep., March of Dimes, Atlanta, GA (2009).

[66] S. Marret, P. Ancel, L. Marpeau, L. Marchand, V. Pierrat, B. Larrogue, Foix-L'Helias, G. Thiriez, J. Fresson, C. Alberge, J. Rose, J. Matis, G. Breart, and M. Kaminski, "Neonatal and 5-Year Outcomes After Birth at 3034 Weeks of Gestation," Obstetrics & Gynecology **110**, 1172 (2007).

[67] J. A. Martin, B. Hamiton, S. Venture, F. Menacker, M. Park, and P. Sutton, "Births: final data for 2001," National Statistics Report **51**, 1–104 (2009).

[68] B. McFarlin, "Quantitative Ultrasound Assessment of the Rat Cervix," Ph.D. thesis, University of Illinois at Chicago (2005).

[69] M. House and S. Socrate, "The cervix as a biomechanical structure," Ultrasound in Obstetrics and Gynecology **28**, 745–749 (2006).

[70] K. M. Myers, A. P. Paskaleva, M. House, and S. Socrate, "Mechanical and biochemical properties of human cervical tissue," Acta Biomaterialia **4**, 104–116 (2008).

[71] B. Timmons, M. Akins, and M. Mahendroo, "Cervical remodeling during pregnancy and parturition," Trends in Endocrinology & Metabolism **21**, 353–361 (2010).

[72] M. House, D. L. Kaplan, and S. Socrate, "Relationships Between Mechanical Properties and Extracellular Matrix Constituents of the Cervical Stroma During Pregnancy," Seminars in Perinatology **33**, 300–307 (2009).

[73] K. Myers, S. Socrate, D. Tzeranis, and M. House, "Changes in the biochemical constituents and morphologic appearance of the human cervical stroma during pregnancy," European Journal of Obstetrics & Gynecology and Reproductive Biology **144, Suppl**, S82–S89 (2009).

[74] C. P. Read, R. A. Word, M. A. Ruscheinsky, B. C. Timmons, and M. S. Mahendroo, "Cervical remodeling during pregnancy and parturition: molecular characterization of the softening phase in mice," Reproduction **134**, 327–340 (2007).

[75] R. M. Aspden, "Collagen Organisation in the Cervix and its Relation to Mechanical Function," Collagen and Related Research **8**, 103–112 (1988).

[76] S. Y. Yu, C. A. Tozzi, J. Babiarz, and P. C. Leppert, "Collagen Changes in Rat Cervix in PregnancyPolarized Light Microscopic and Electron Microscopic Studies," Proceedings of the Society for Experimental Biology and Medicine. Society for Experimental Biology and Medicine (New York, N.Y.) **209**, 360–368 (1995).

[77] M. L. Akins, K. Luby-Phelps, and M. Mahendroo, "Second harmonic generation imaging as a potential tool for staging pregnancy and predicting preterm birth," Journal of Biomedical Optics **15**, 26020 (2010).

[78] Y. Zhang, M. L. Akins, K. Murari, J. Xi, M.-J. Li, K. Luby-Phelps, M. Mahendroo, and X. Li, "A compact fiber-optic SHG scanning endomicroscope and its application to visualize cervical remodeling dur-

ing pregnancy." Proceedings of the National Academy of Sciences of the United States of America **109**, 12878–83 (2012).

[79] N. I. Fisher, *Statistical analysis of circular data* (Cambridge University Press, Cambridge, 1993), 1st ed.

[80] S. Rao Jammalamadaka Ambar Sengupta, *Topics in Circular Statistics* (World Scientific, Singapore, 2001).